Cyclic GMP Diffusion Coefficient in Rod Photoreceptor Outer Segments

Y. Koutalos,* K. Nakatani,‡ and K.-W. Yau,*§†

*Departments of Neuroscience and †Ophthalmology and § Howard Hughes Medical Institute, The Johns Hopkins University School of Medicine, Baltimore, Maryland 21205 USA, and ‡ Institute of Biological Sciences, University of Tsukuba, Tsukuba, Ibaraki 305, Japan

ABSTRACT Cyclic GMP (cGMP) is the intracellular messenger that mediates phototransduction in retinal rods. As photoisomerizations of rhodopsin molecules are local events, the longitudinal diffusion of cGMP in the rod outer segment should be a contributing factor to the response of the cell to light. We have employed the truncated rod outer segment preparation from bullfrog (*Rana catesbeiana*) and tiger salamander (*Ambystoma tigrinum*) to measure the cGMP diffusion coefficient. In this preparation, the distal portion of a rod outer segment was drawn into a suction pipette for measuring membrane current, and the rest of the cell was then sheared off with a glass probe, allowing bath cGMP to diffuse into the outer segment and activate the cGMP-gated channels on the surface membrane. Addition and removal of bath cGMP were fast enough to produce effectively step changes in cGMP concentration at the open end of the outer segment. When cGMP hydrolysis is inhibited by isobutylmethylxanthine (IBMX), the equation for the diffusion of cGMP inside the truncated rod outer segment has a simple analytical solution, which we have used to analyze the rise and decay kinetics of the cGMP-elicited currents. From these measurements we have obtained a cGMP diffusion coefficient of $\sim 70 \times 10^{-8}$ cm^2 s^{-1} for bullfrog rods and $\sim 60 \times 10^{-8}$ cm^2 s^{-1} for tiger salamander rods. These values are six to seven times lower than the expected value in aqueous solution. The estimated diffusion coefficient is the same at high (20–1000 μM) and low (5–10 μM) concentrations of cGMP, suggesting no significant effect from buffering over these concentration ranges.

INTRODUCTION

Visual transduction takes place in the outer segments of retinal rod and cone photoreceptors. Compared with cones, the rods have been much more extensively studied. They mediate vision at low light intensities and can detect light down to a single photon. The rod outer segment is cylindrical in shape, and along its entire length there are a large number (~1000) of completely internalized membranous disks stacked on top of each other (see, for example, Rodieck, 1973). These disks contain the photosensitive pigment rhodopsin, which is a transmembrane protein. Phototransduction is initiated when photons are absorbed by the rhodopsin molecules. This signal transduction process involves a G protein-mediated enzyme cascade that leads to stimulation of a cyclic GMP (cGMP)-phosphodiesterase complex and the consequent hydrolysis of cGMP (for recent reviews, see Lagnado and Baylor, 1992; Detwiler and Gray-Keller, 1992; Pugh and Lamb, 1993; Koutalos and Yau, 1993; Yau, 1994). In the dark, cytoplasmic cGMP binds to and opens cGMP-activated cation channels on the plasma membrane of the outer segment, maintaining an inward current (for review, see Yau and Baylor, 1989). In the light, the level of cGMP falls, resulting in closure of the cGMP-activated channels and hence a membrane hyperpolarization, which constitutes the electrical response to light. Recovery from light involves the decays of the active intermediates in the phototransduction cascade, with the restoration of the dark cGMP concentration effected by the activity of guanylate cyclase, the cGMP-synthesizing enzyme (see above reviews).

The activation of a rhodopsin molecule by a photon and the subsequent stimulation of the phosphodiesterase are local events, being confined to a single disk surface. On the other hand, one photon is known to suppress 3–5% of the dark current (Baylor et al., 1979b), indicating that the photoexcitation must spread over a minimum distance spanning 30–50 disks. Thus, the longitudinal diffusion of cGMP in the outer segment should be a determinant of the spread of the light response and, consequently, of the sensitivity of the cell to light. This diffusion of cGMP in the outer segment ought to be slower than in aqueous solution due to the baffling effect of the disks. At the same time, if there are cGMP binding sites in the outer segment that rapidly buffer free cGMP, the cGMP diffusion may be slowed further. Estimation of the cytoplasmic free cGMP concentration from the fraction of cGMP-gated channels open in the dark has suggested that this pool represents only up to a few percent of the total (Nakatani and Yau, 1988b).

The first quantitative study of the spread of photoexcitation along the rod outer segment was carried out by Lamb et al. (1981), who estimated an upper bound of $\sim 30 \times 10^{-8}$ cm^2 s^{-1} for the diffusion coefficient of the internal messenger mediating phototransduction. However, this estimate was indirect, relying on an empirical description of the photoexcitation process. More recently, Cameron and Pugh (1990) estimated an upper limit of 10×10^{-8} cm^2 s^{-1} for the cGMP diffusion coefficient, by infusing cGMP and 8-Bromo-cGMP into a rod cell through a whole cell pipette and recording the elicited membrane current. Olson and Pugh (1993) arrived at a similar upper limit by infusing a fluorescent cGMP analogue into a rod outer segment and measuring the spread of fluorescence.

Received for publication 3 June 1994 and in final form 17 October 1994.

Address reprint requests to Dr. Yiannis Koutalos, Department of Neuroscience, 900 PCTB, 725 N. Wolfe St., Baltimore, MD 21205. Tel.: 910-955-1261.

0006-3495/95/01/373/10 $2.00

Considering the importance of this parameter for an ultimately quantitative understanding of the phototransduction process, we have undertaken a new measurement of the cGMP diffusion coefficient in the rod outer segment by using the truncated rod outer segment preparation (Yau and Nakatani, 1985; Nakatani and Yau, 1988b). With this preparation, we dialyzed cGMP into an open-ended rod outer segment and used the cGMP-gated channels on the plasma membrane of the outer segment to monitor the internal cGMP concentration. From the rise and decay kinetics of the membrane current elicited by step changes in the bath cGMP concentration, the diffusion coefficient of cGMP could be estimated. The estimate we arrived at is several times higher than those in the previous studies.

MATERIALS AND METHODS

Bullfrogs, *Rana catesbeiana*, and larval tiger salamanders, *Ambystoma tigrinum*, (both from Charles D. Sullivan, Nashville, TN) were decapitated and pithed under dim red light. All subsequent procedures were performed in infrared light with the help of image converters. The enucleated eyes were hemisected, and the retinas were isolated and kept at room temperature for up to several hours in Ringer's solution containing (in mM): 110 NaCl, 2.5 KCl, 1.6 $MgCl_2$, 1 $CaCl_2$; 5 TMA-HEPES (tetramethylammonium hydroxide-4-(2-hydroxyethyl)1-piperazineethanesulfonic acid), 5 glucose, pH 7.55. Single, isolated rod cells were obtained by chopping a piece of retina, under Ringer's solution, with a razor blade in a petri dish coated with Sylgard elastomer (Dow Corning, Midland, MI).

Suction pipettes for recording membrane current from rod outer segments were made from Corning 7740 borosilicate glass capillaries (A-M Systems, Everett, WA) and coated with tri-*n*-butylchlorosilane (Pfaltz and Bauer, Waterbury, CT), as described previously (Baylor et al., 1979a; Lamb et al., 1981). A truncated rod outer segment was obtained by drawing the outer segment of a rod cell partially into a suction pipette and then shearing off the remainder of the cell with a glass probe made from the same capillaries (Fig. 1). The membrane potential was held at 0 mV. This preparation allows both recording of membrane current from the outer segment and internal dialysis of the outer segment with the bath solution (Yau and Nakatani, 1985; Nakatani and Yau, 1988b). In most of the experiments, the suction pipette was filled with Ringer's solution, and a pseudointracellular bath solution (in mM: 12.5 NaCl, 100 potassium gluconate, 1.6 $MgCl_2$, 5 TMA-HEPES, 5 glucose, pH 7.55) containing 0.5 mM isobutylmethylxanthine (IBMX) and different concentrations of cGMP was used for dialysis. The IBMX served to inhibit any cGMP-phosphodiesterase activity in the outer segment. With this solution arrangement, the membrane current was inward, being carried by Na^+ from the pipette solution. In a few experiments, a different solution arrangement, with low Ca^{2+} in the pipette and negligible Na^+ in the bath, was adopted to avoid any contamination of the recorded cGMP-activated current from electrogenic $Na^+/Ca^{2+},K^+$ exchange activity (Yau and Nakatani, 1984; Cervetto et al., 1989). This solution arrangement consisted of a choline pipette solution (in mM: 110 choline chloride, 0.5 $MgCl_2$, 2 1,2-bis(*o*-aminophenoxy)ethane-*N*,*N*,*N'*,*N'*-tetraacetic acid (BAPTA), 1.79 $CaCl_2$ (0.001 free Ca^{2+}), 5 TMA-HEPES, 5 glucose, pH 7.55) and a potassium gluconate bath solution (in mM: 110 potassium gluconate, 0.5 $MgCl_2$, 5 TMA-HEPES, 5 glucose, pH 7.55) containing 0.5 mM IBMX. In this case, the current was outward, being carried by K^+ from the dialysis solution. In certain experiments, 100 μM $NiCl_2$ was also present in the bath solution, or IBMX was omitted. Changes of bath solution were effected by a system of pneumatically controlled valves and were complete around the outer segment within ~300 ms (Nakatani and Yau, 1988a).

All reagents were of analytical grade. The experiments were carried out in darkness and at room temperature. Electrical records were low-pass filtered at 10–30 Hz. In all of the figures, inward membrane current is plotted as a negative current.

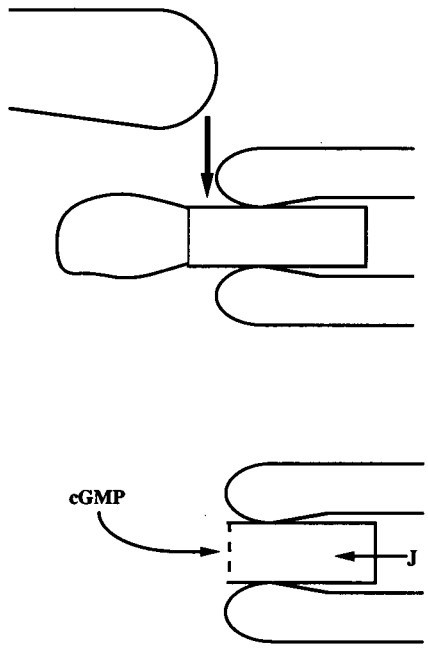

FIGURE 1 Diagram illustrating the truncated rod outer segment preparation.

THEORY

Absence of cGMP hydrolysis

Fig. 2 is a schematic diagram of a truncated rod outer segment preparation. We expect the diffusion of cGMP to be much faster laterally than longitudinally, because the baffling from the membranous disks impedes only longitudinal diffusion. Thus, we can assume cross-sectional homogeneity

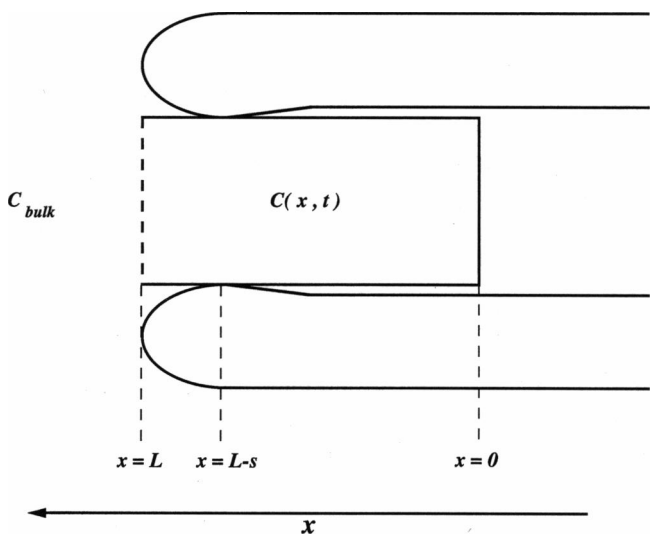

FIGURE 2 Schematic diagram of a truncated rod outer segment for the construction of the one-dimensional diffusion model. The distal, closed end of the outer segment is at $x = 0$, whereas the proximal, open end is at $x = L$. $C(x,t)$ is the cGMP concentration at distance x from the closed end and at time t. C_{bulk} is the concentration of cGMP in the bath.

in the time scale of longitudinal diffusion, and the problem reduces to a one-dimensional one. In the absence of hydrolysis, as would be the case with IBMX present in the dialyzing solution, the concentration, $C(x, t)$, of cGMP at distance x and time t satisfies the diffusion equation:

$$\frac{\partial C(x, t)}{\partial t} = D \frac{\partial^2 C(x, t)}{\partial x^2} \tag{1}$$

where D is the diffusion coefficient.

Two situations to consider are: (1) the bath cGMP concentration is switched from 0 to C_0, and (2), the bath cGMP concentration is switched from C_0 to 0. Because the bath solution change took less than 300 ms to complete (see Materials and Methods), compared with several seconds required for cGMP in the outer segment to reach equilibrium (see Results), the change in cGMP concentration at the open end of the outer segment can be considered to be instantaneous. For the switching on of cGMP, the boundary conditions are:

$$\frac{\partial C}{\partial x}(0, t) = 0 \tag{2}$$

$$C(L, t) = C_0 \tag{3a}$$

and the initial condition is:

$$C(x, 0) = 0 \tag{4a}$$

For the switching off of cGMP, the boundary condition at $x = 0$ is the same, being described by Eq. 2, whereas that at $x = L$ is:

$$C(L, t) = 0 \tag{3b}$$

The corresponding initial condition is:

$$C(x, 0) = C_0 \tag{4b}$$

Eq. 2 reflects the zero-flux requirement at the closed end of the outer segment, whereas Eqs. 3a and 3b reflect the bath cGMP concentration at the open end under the two conditions. Eqs. 3a and 3b are applicable in the absence of a significant unstirred layer between the open end of the outer segment and the bulk solution. Otherwise, the appropriate boundary condition becomes, in the first situation, for example:

$$\frac{\partial C}{\partial x}(L, t) = h(C_0 - C(L, t)) \tag{3'a}$$

where h is a constant inversely proportional to the thickness of the unstirred layer. In this case Eq. 1 has an analytical solution (see Carslaw and Jaeger, 1959, p. 122, Eq. 12), which we used to analyze the effect of an unstirred layer on our diffusion coefficient estimates. In experiments with the dye neutral red in the pipette, an unstirred layer was visually undetectable, placing an upper limit of ~5 μm for its thickness. With an unstirred layer of this thickness, the analysis yields the same diffusion coefficient value as in its absence. An unstirred layer made a significant difference only if the thickness was greater than the length of the truncated outer segment, i.e., at least 20 μm. Because this is much larger than the upper limit from the neutral red experiments, we have used Eqs. 3a and 3b for boundary conditions.

The solution of Eq. 1 subject to conditions 2, 3a, and 4a is given in Carslaw and Jaeger (1959, p. 101, Eq. 5):

$$C(x, t) = C_0 - \frac{4C_0}{\pi} \sum_{m=0}^{\infty} \left\{ \frac{(-1)^m}{(2m + 1)} \times \exp\left(- \frac{(2m + 1)^2 \pi^2 Dt}{4L^2} \right) \cos \frac{(2m + 1)\pi x}{2L} \right\} \tag{5a}$$

Similarly, the solution of Eq. 1 subject to conditions 2, 3b, and 4b is:

$$C(x, t) = \frac{4C_0}{\pi} \sum_{m=0}^{\infty} \left\{ \frac{(-1)^m}{(2m + 1)} \times \exp\left(- \frac{(2m + 1)^2 \pi^2 Dt}{4L^2} \right) \cos \frac{(2m + 1)\pi x}{2L} \right\} \tag{5b}$$

Introducing the dimensionless variables X and T:

$$X = \frac{x}{L} \tag{6}$$

$$T = \frac{Dt}{L^2} \tag{7}$$

we get, from Eqs. 5a and 5b:

$$C(X, T) = C_0 - \frac{4C_0}{\pi} \sum_{m=0}^{\infty} \left\{ \frac{(-1)^m}{(2m + 1)} \times \exp\left(- \frac{(2m + 1)^2 \pi^2 T}{4} \right) \cos \frac{(2m + 1)\pi X}{2} \right\} \tag{8a}$$

$$C(X, T) = \frac{4C_0}{\pi} \sum_{m=0}^{\infty} \left\{ \frac{(-1)^m}{(2m + 1)} \times \exp\left(- \frac{(2m + 1)^2 \pi^2 T}{4} \right) \cos \frac{(2m + 1)\pi X}{2} \right\} \tag{8b}$$

Eqs. 8a and 8b can be evaluated for different values of X and T independent of the diffusion coefficient value and the outer segment length. Furthermore, the infinite series converges rapidly, with the first few terms providing a good approximation (see Carslaw and Jaeger, 1959). We have kept the first six terms in our numerical calculations.

We have to relate the cGMP concentration, C, to the outer segment current, J, recorded by the suction pipette. This current is collected from the part of the outer segment distal to the seal between pipette and cell membrane. Empirically, the relation between J and C is described fairly well by the Hill equation:

$$J = J_{max} \frac{C^n}{C^n + K_{1/2}^n} \tag{9}$$

where J_{max} is the saturated current elicited at high cGMP concentrations, and $K_{½}$ and n are the half-activating cGMP concentration and the Hill coefficient, respectively (see Results).

The cGMP-gated channels are distributed uniformly along the length of the outer segment (Baylor et al., 1979a;

Nakatani and Yau, 1988b). Assuming a homogeneous population of channels, and using the dimensionless variables, the current $dJ(X, T)$ elicited from the length dX at (X, T) by the concentration $C(X, T)$ is then given by:

$$dJ(X, T) = J_{max} \frac{C^n(X, T)}{C^n(X, T) + K_{1/2}^n} dX \tag{10}$$

and the current collected by the suction pipette is:

$$J(T) = J_{max} \int_0^u \frac{C^n(X, T)}{C^n(X, T) + K_{1/2}^n} dX \tag{11}$$

where $u = 1 - s/L$ (see Fig. 2).

In previous work, the value of s was estimated to be 5–20 μm (Nakatani and Yau, 1988b). We have performed one experiment to measure s in this study and obtained a value of ~5 μm. The value for s, however, does not significantly affect the determination of the diffusion coefficient. From Eq. 11, it can be seen that the dependence on s is through the ratio s/L. For a rather high s/L ratio of 0.9 (i.e., when current is collected only from the distal 10% of the outer segment length), the estimated diffusion coefficient would be only ~50% larger than that for a ratio of 0 (i.e., when current is collected from the full outer segment length). This is less than the dispersion of the measured values from the same cell (see Results). We have adopted $s = 5$ μm in all subsequent analyses. With Eqs. 8a or 8b and 11, $J(T)$ can be evaluated for each truncated rod outer segment and fitted to the observed current time course obtained upon changing bath cGMP. For fitting, the template $J(T)$ is scaled on the time axis to match the experimental record in real time, $J(t)$:

$$J(t) = J\left(\frac{T}{\alpha}\right) \tag{12}$$

where α is the scaling factor. From Eq. 7:

$$D = \alpha L^2 \tag{13}$$

which allows the diffusion coefficient D to be evaluated. D can also be obtained from collected results as the slope of the plot of α versus $1/L^2$.

One concern is the possibility of a space-clamp failure in our experiments that would diminish current collection from the distal part of the outer segment, hence skewing the apparent diffusion coefficient to higher values. This problem seems unlikely for the following reasons. First, the cGMP-elicited current scales linearly with the length of the truncated outer segment (Nakatani and Yau, 1988b), which is inconsistent with the above concern. Second, the current kinetics depend mostly on the kinetics of cGMP diffusion rather than the length of outer segment contributing current. As an extreme example, for an outer segment 60 μm long, but with the distal 30 μm not contributing any current at all, it can be calculated that the diffusion coefficient would be overestimated by no more than a factor of 2, which is less than the variability in scaling factor obtained in a given experiment. Finally, the values of diffusion coefficient we obtained did not vary consistently with the length of the truncated outer segment or the longitudinal current density (such as in experiments involving different concentrations of cGMP), contrary to what would be expected from any space-clamp problem.

Presence of cGMP hydrolysis

A concern with the above approach for the determination of the cGMP diffusion coefficient is that the experiments have to be carried out in the presence of IBMX, which is essential for the inhibition of hydrolysis by the cGMP-phosphodiesterase. It is conceivable that IBMX might interfere with the diffusion of cGMP inside the rod outer segment, such as by occupying cGMP binding sites that would otherwise slow down diffusion. We have attempted to address this issue by carrying out experiments in the absence of IBMX. In this case the cGMP-phosphodiesterase is active. At cGMP concentrations low enough so that the phosphodiesterase operates in the linear range, Eq. 1 can be modified to account for hydrolysis:

$$\frac{\partial C(x, t)}{\partial t} = D \frac{\partial^2 C(x, t)}{\partial x^2} - \beta C(x, t) \tag{1'}$$

where β is the hydrolytic rate of the phosphodiesterase. The solutions of this equation for the switching on and off of bath cGMP can be derived from Eqs. 5a and 5b according to Carslaw and Jaeger (1959, Eqs. 21–25, pp. 32–33). For the switching on of cGMP, the boundary and initial conditions are again given by Eqs. 2, 3a, and 4a. For the switching off of cGMP, the boundary conditions are the same, but the initial condition becomes:

$$C(x, 0) = f(x) = C_0 \frac{\cosh(\sqrt{\beta/D}x)}{\cosh(\sqrt{\beta/D}L)} \tag{4'b}$$

This equation describes the steady-state cGMP gradient along the outer segment in the presence of hydrolysis.

The solutions of Eq. 1′ for the two cases are, respectively:

$$C(x, t) = f(x) - \frac{4C_0}{\pi} \exp(-\beta t) \times \sum_{m=0}^{\infty} \left\{ \frac{(-1)^m (2m + 1)(\pi^2 D/4L^2)}{\beta + (2m + 1)^2(\pi^2 D/4L^2)} \times \exp\left(-\frac{(2m + 1)^2 \pi^2 Dt}{4L^2}\right) \cos\frac{(2m + 1)\pi x}{2L} \right\} \tag{5'a}$$

$$C(x, t) = e^{-\beta t} \sum_{m=0}^{\infty} \left\{ \exp\left(-\frac{(2m + 1)^2 \pi^2 Dt}{4L^2}\right) \times \cos\frac{(2m + 1)\pi x}{2L} \left(\int_0^L f(z) \cos\frac{(2m + 1)\pi z}{2L} dz \right) \right\} \tag{5'b}$$

These equations cannot be transformed into the equivalents of

Eqs. 8a and 8b, so Eq. 11 also cannot be used. Instead, we have to use:

$$J(t) = \frac{J_{max}}{L - s} \int_0^{L-s} \frac{C^n(x, t)}{C^n(x, t) + K_{1/2}^n} dx \qquad (11')$$

Apart from the lack of templates for $J(T)$, the $J(t)$ as given by Eq. 11′ has the disadvantage of being highly sensitive to the value of s. The reason for this high sensitivity is the steep drop of the cGMP concentration inside the outer segment due to hydrolysis. In addition, because of cGMP hydrolysis, the values for the constants $K_{1/2}$ and n cannot be determined in the same outer segment as the kinetic measurements. Instead, averages of measurements from other rod outer segments in the absence of hydrolysis would have to be used. All of these considerations together rule out an accurate determination of the diffusion coefficient in the presence of cGMP hydrolysis. Nevertheless, we have carried out a few of these experiments. Although we shall not describe these experiments here, the results did not show any obvious inconsistency with the diffusion coefficient values arrived at in the presence of IBMX.

RESULTS

Fig. 3 shows membrane current recordings from a truncated bullfrog rod outer segment, with a length L within the pipette of 60 μm. In this experiment, the suction pipette contained Ringer's solution, and the bath a pseudointracellular solution (see Methods). The inward cGMP-elicited currents were produced by step changes of cGMP in the bath, in the presence of IBMX. J_{max}, ~200 pA for this experiment, was elicited with 1 mM cGMP, a concentration high enough to saturate the channels (see Nakatani and Yau, 1988b). The current induced by this high cGMP concentration often showed a transient outward component (or decrease of the inward current) at its peak (Fig. 3). The underlying cause of this component is unknown, but it cannot be Na^+/Ca^{2+}, K^+ exchange activity, which would give rise to a current in the inward direction. The relation between steady-state current and cGMP concentration from this experiment is shown in Fig. 4. The smooth curve fitted to the experimental points is Eq. 9, with $K_{1/2}$ and n values of 80 μM and 2.17, respectively.

From the specified values of $K_{1/2}$, n, J_{max}, and L, $J(T)$ templates can be constructed for the rising and falling phases of the cGMP-elicited currents in Fig. 3 by using Eqs. 8a, 8b, and 11. The templates for 100 μM bath cGMP are shown in Fig. 5*A* and *B*, and their scaled fits to the recorded current $J(t)$ are shown in Fig. 5*C*. The scaling factor α is 0.022 s^{-1} for both the rising and the falling phases. Fig. 6 shows similar fittings for the currents in Fig. 3 elicited by 50 μM, 25 μM, and 1 mM cGMP, with the α values given in the figure legend. We have not analyzed the current rising phase for the 1 mM cGMP exposure because the early saturation of the current limits the resolution and because of the transient outward current at its peak. In Fig. 6*C*, the template (curve 1) does not reproduce the current falling phase very well, but one with an s value of 15 μm and the same α value does much better (curve 2). Such a discrepancy between the shape of the template and the experimental record is generally evident only for the 1 mM bath cGMP withdrawals, due to the saturation of the channels giving rise to a salient plateau. At lower cGMP concentrations, such shape differences were not sufficiently pronounced to be resolved. In general, the templates could reproduce the shape of the experimental record by adjusting the seal position and by adding an unstirred layer of reasonable thickness. However, as pointed out before (see Theory), neither of these two adjustments (seal position and unstirred layer) has a significant influence on the value of the diffusion coefficient. The latter is more related to the overall excursion time for the current decline or rise.

The scaling factors for the rising and the falling phase at a given cGMP concentration are not always identical, such

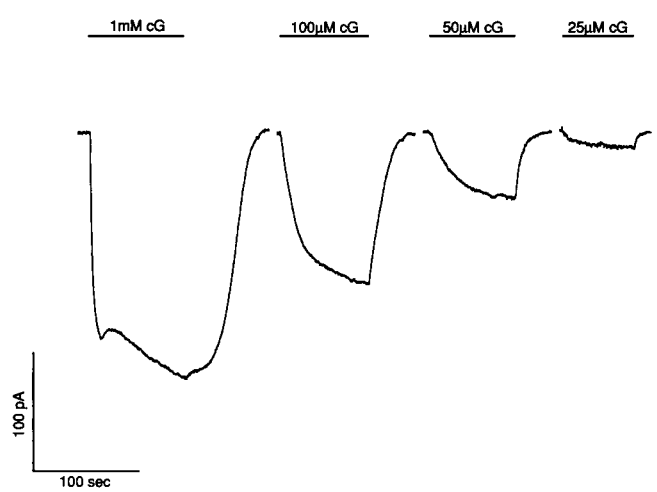

FIGURE 3 Membrane currents induced by different concentrations of cGMP from a truncated bullfrog rod outer segment. The pipette contained Ringer's solution. L = 60 μm.

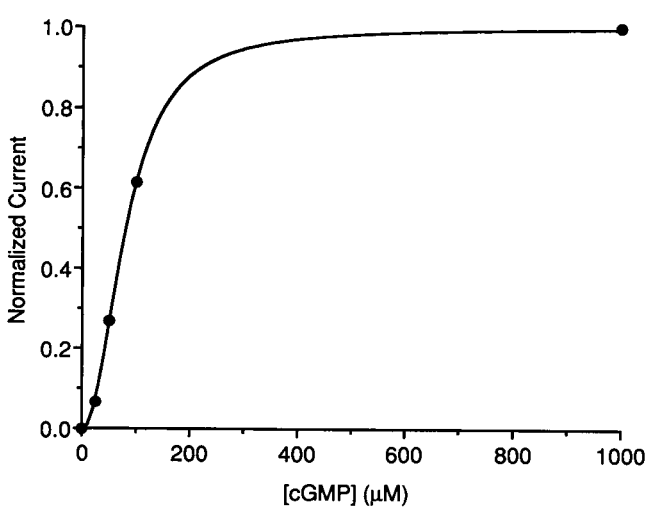

FIGURE 4 Relation between steady-state current and cGMP concentration for the experiment of Fig. 3. The currents have been normalized with respect to that at 1 mM cGMP. The smooth curve is the Hill equation (Eq. 9) with $K_{1/2}$ = 80 μM and n = 2.17.

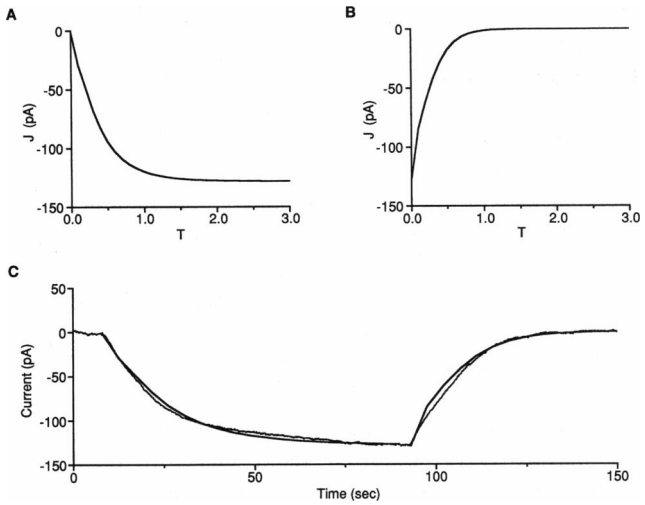

FIGURE 5 (*A*) $J(T)$ template for the rising phase of the current elicited by 100 μM cGMP, calculated from Eqs. 8a and 11, with $K_{1/2}$ = 80 μM, n = 2.17, and s = 5 μm. (*B*) $J(T)$ template for the falling phase of the current elicited by 100 μM cGMP, calculated from Eqs. 8b and 11, with the same parameters. (*C*) Scaled fits of the templates (thick lines) to the current record (thin line) for the 100 μM cGMP step in Fig. 3. The scaling factor α is 0.022 s^{-1} for both the rising and falling phase.

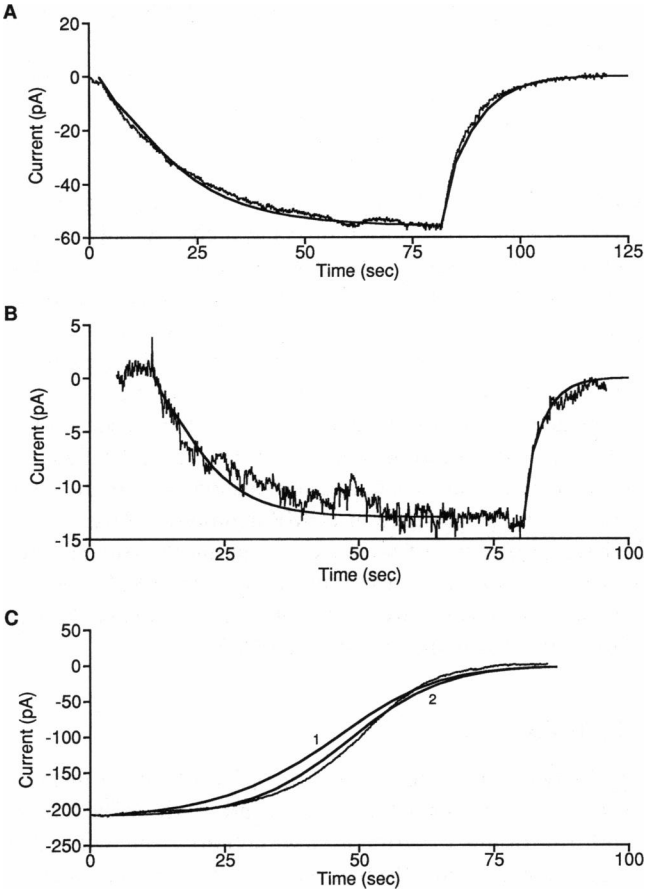

FIGURE 6 $J(T)$ template fittings to the currents in Fig. 3 elicited by 50 μM (*A*), 25 μM (*B*), and 1 mM (*C*) cGMP. Same procedure as in Fig. 5. The α value is 0.027 s^{-1} for the rising phase and 0.060 s^{-1} for the falling phase in (*A*) and 0.055 s^{-1} for both the rising and the falling phase in (*B*). In (*C*), curves 1 and 2 are falling-phase templates constructed with s = 5 μm and s = 15 μm, respectively; α is 0.023 s^{-1} for both.

as the case for the 50 μM cGMP experiment in Fig. 6*A* (see legend). The difference between the two scaling factors, however, is not systematic across experiments. The presence of an appreciable hydrolytic activity would have, for example, resulted in current kinetics with a rising phase consistently slower than the falling phase. This absence of significant cGMP-phosphodiesterase activity is expected from the presence of 0.5 mM IBMX. From the fittings shown in Figs. 5*C* and 6, *A–C* (altogether seven determinations), we obtain an average α value of 0.037 $\pm$ 0.017 s^{-1} (mean $\pm$ SD). From Eq. 13 and L = 60 μm, we get D = 133 $\pm$ 61 $\times$ 10^{-8} cm^2 s^{-1}.

The inverse relation between α and L^2 according to Eq. 13 is directly demonstrated by the experiment of Fig. 7, which was carried out on the same outer segment as in Fig. 3. In panel *A*, traces 1–4 correspond to the current declines upon switching off 1 mM bath cGMP at L values of 60, 50, 40, and 32 μm, respectively. The different lengths were obtained by pushing the outer segment out of the suction electrode by different amounts and following with retruncation. The traces have been normalized to the same amplitude and synchronized with respect to the time of switching off bath cGMP (time 0). As expected, the shorter the outer segment length, the faster was the current decay. In Fig. 7*B*, the α values used for fitting the $J(T)$ templates to the traces are plotted against $1/L^2$. The slope of a straight line fitted to the points and passing through the origin gives a D value of 54 $\pm$ 4 $\times$ 10^{-8} cm^2 s^{-1} (the error is calculated from the least-squares fit).

To average over all experiments, we made a collected plot of α versus $1/L^2$ (Fig. 8). Typically, we have estimated the scaling factors by matching the mid or 90% completion point of a template to the real time record. Both methods of comparison gave similar results. Fig. 8*A* shows collected results from bullfrog rod outer segments, all with Ringer's solution in the pipette. A straight-line fit to the points and through the origin gives D = 69 $\pm$ 8 $\times$ 10^{-8} cm^2 s^{-1}. Fig. 8*B* shows collected results from another group of bullfrog rods, with choline solution in the pipette (see Materials and Methods), which gives D = 54 $\pm$ 5 $\times$ 10^{-8} cm^2 s^{-1}. Finally, Fig. 9 shows collected results from similar experiments on tiger salamander rods, all with Ringer's solution in the pipette. They give a D value of 56 $\pm$ 6 $\times$ 10^{-8} cm^2 s^{-1}, not significantly different from that in bullfrog rods. Because salamander rods have shorter outer segments than bullfrog rods, the range of L values covered in these experiments was smaller. Table 1 summarizes the estimates according to species and experimental condition. In Figs. 8 and 9, there is considerable scatter of the data points around the least-squares lines. However, the deviations appear to be random rather than systematic. Specific concerns about space-clamp failure are already dealt with in the Theory section.

In the above experiments, the analysis of the current time course was generally limited to cGMP concentrations above ~20 μM, because of the rapid decrease in current amplitude

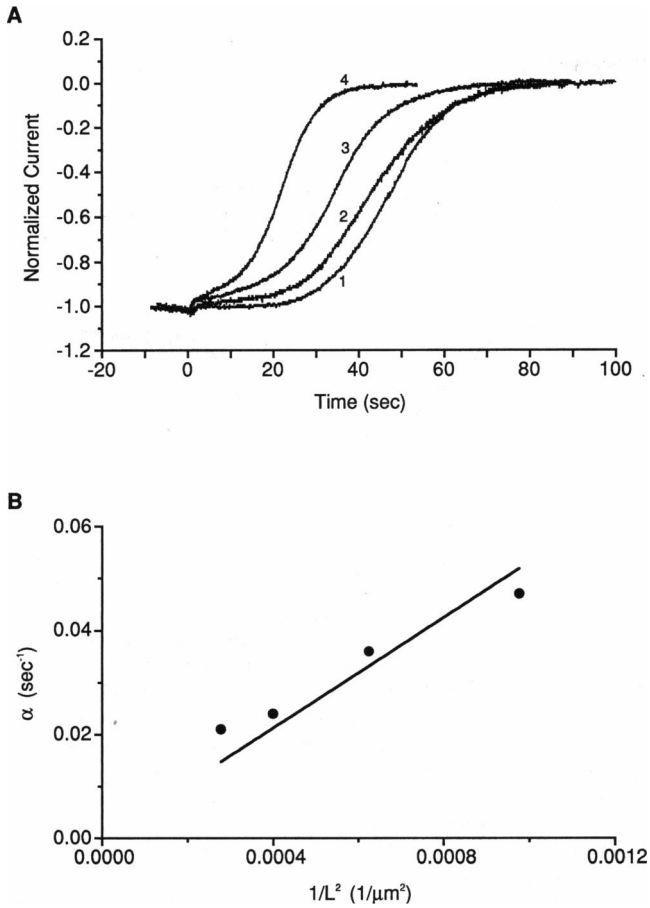

FIGURE 7 (*A*) Decline of the current elicited by 1 mM cGMP with different outer segment length, *L*, within the suction pipette. Same cell as in Fig. 3. The traces have been normalized to the same initial amplitude and synchronized to facilitate comparison. The numbers 1, 2, 3, and 4 correspond to L = 60, 50, 40, and 32 μm, respectively. The $J(T)$ template fittings to these falling phases gave scaling factors of 0.021 s^{-1}, 0.024 s^{-1}, 0.036 s^{-1}, and 0.047 s^{-1}, respectively. (*B*) The scaling factor α obtained from panel *A* plotted as a function of $1/L^2$. The straight line is a least-squares fit constrained to pass through the origin, with its slope giving a diffusion coefficient D of 54 ± 4 × 10^{-8} cm^2 s^{-1}.

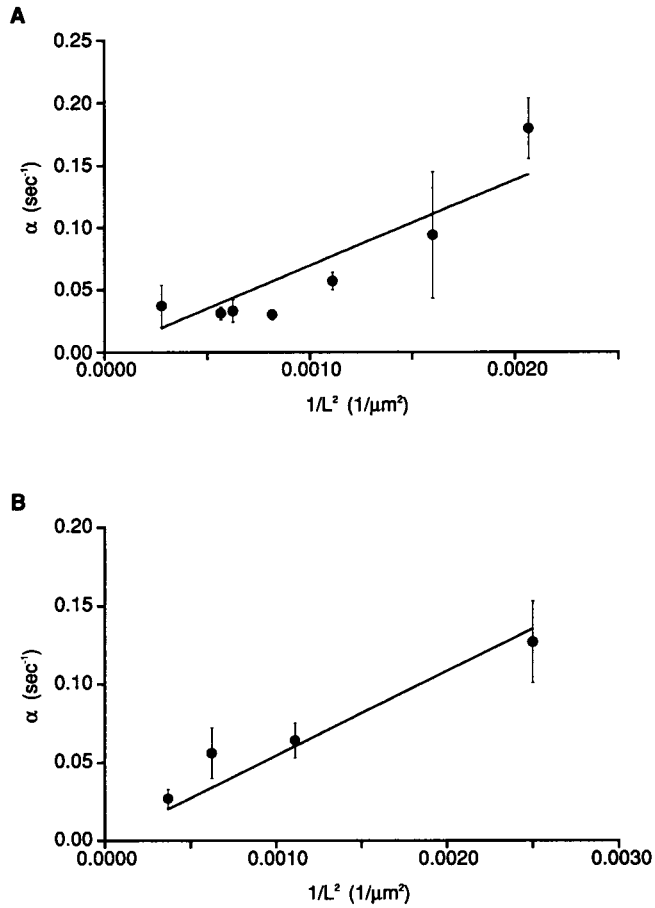

FIGURE 8 (*A*) Collected results from different bullfrog rod outer segments, with Ringer's solution in the pipette in all cases. Each point represents averaged measurements from one outer segment, with the numbers of α determinations being, from left to right, 7, 5, 5, 4, 7, 4, 7. The straight line is a least-squares fit passing through the origin, with a slope D of 69 ± 8 × 10^{-8} cm^2 s^{-1}. (*B*) Collected results from another set of bullfrog experiments, but with choline chloride solution in the pipette. Each point represents the α value from a single cell and is the average of four determinations. The slope of the line is D = 54 ± 5 × 10^{-8} cm^2 s^{-1}.

with decreasing cGMP concentration (see, for example, Fig. 3). However, because the physiological cGMP concentration is considered to be less than 10 μM (Nakatani and Yau, 1988b), it is relevant to try to determine the diffusion coefficient at such low cGMP concentrations. This measurement is particularly important if buffering slows down cGMP diffusion at low cGMP concentrations. To measure the diffusion coefficient at low cGMP concentrations, the sensitivity of the channel to cGMP has to be increased. We achieved this by including in the dialyzing solution 100 μM Ni^{2+}, a cation known to increase the apparent affinity of the channel for cGMP (Karpen et al., 1993). We found that 100 μM Ni^{2+} shifted the $K_{1/2}$ value to ~10 μM for both bullfrog and salamander rods, with a Hill coefficient between 2 and 4. After determining the $K_{1/2}$ and n values in a dose-response experiment in the presence of Ni^{2+}, the diffusion coefficient could be estimated in the same way as described above. Furthermore, in this kind of experiment, the diffusion coefficients at high and low cGMP concentrations could be compared in the same outer segment, by first carrying out measurements at high cGMP concentrations in the absence of Ni^{2+} and then repeating the measurements at low cGMP concentrations after a transient (~5 min) exposure to 100 μM Ni^{2+}. This experimental protocol is possible because Ni^{2+} remains associated with the channel for at least 10 min in the absence of Ni^{2+}-chelating agents (Karpen et al., 1993). Fig. 10*B* shows the current kinetics elicited from a bullfrog rod outer segment by switching on and off 5 μM cGMP in the bath solution, after exposure to 100 μM Ni^{2+}. The curves fitted to the experimental trace are $J(T)$ templates with α values of 0.058 s^{-1} and 0.050 s^{-1} for the rising and the falling phase, respectively. The outer segment length was L = 25 μm, giving diffusion coefficients of 36 × 10^{-8} cm^2 s^{-1} and 31 × 10^{-8} cm^2 s^{-1}, respectively. The measurements were repeated with 10 μM cGMP (data not shown), giving an overall average value (four determinations) for D of

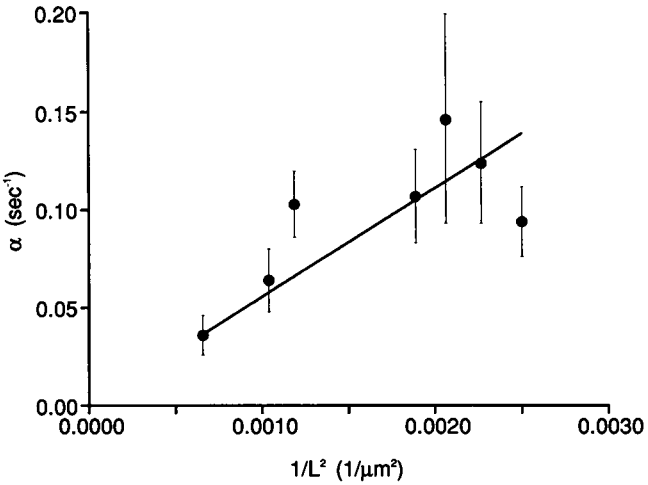

FIGURE 9 Collected results from larval tiger salamander rod outer segments, with Ringer's solution in the pipette in all cases. Each point represents the averaged α value from a single outer segment, with the numbers of determinations being, from left to right: 7, 4, 7, 7, 7, 7, 4. The slope of the line is $D = 56 \pm 6 \times 10^{-8}$ cm^2 s^{-1}.

TABLE 1 Longitudinal diffusion coefficient for cGMP measured from bullfrog and salamander rod outer segments

Species	cGMP diffusion coefficient ($\times 10^{-8}$ cm^2 s^{-1})
Bullfrog (Ringer's)	69 ± 8
Bullfrog (choline)	54 ± 5
Salamander (Ringer's)	56 ± 6

The values are from the slopes of the straight line fits in Figs. 8 and 9. The pipette solution for each set of experiments is given in parentheses.

$39 \pm 9 \times 10^{-8}$ cm^2 s^{-1}. In comparison, the diffusion coefficient obtained from the same outer segment with 20 and 35 μM cGMP steps before the exposure to Ni^{2+} was $56 \pm 28 \times 10^{-8}$ cm^2 s^{-1} (four determinations), which is not significantly different. The current trace with fitted templates for 35 μM cGMP is shown in Fig. 10*A*.

Table 2 summarizes the comparison of diffusion coefficients at high and low cGMP concentrations from tiger salamander and bullfrog rod outer segments. The agreement between the numbers at high and low cGMP concentrations suggests an absence of rapid buffering of cGMP in the rod outer segments over the concentration range of 5 μM to 1 mM.

DISCUSSION

The diffusion coefficient of several nucleotides, including AMP, in aqueous solution near physiological ionic strength has been measured to be $\sim 4 \times 10^{-6}$ cm^2 s^{-1} (Bowen and Martin, 1964). This is six to seven times higher than the 50 to 70 $\times 10^{-8}$ cm^2 s^{-1} we have measured for cGMP in the rod outer segment. Previously, measurements in molluscan neurons have given a cAMP diffusion coefficient of 3.3×10^{-6} cm^2 s^{-1} (Huang and Gillette, 1991). A major factor in the lowering of the longitudinal diffusion coefficient in rod outer

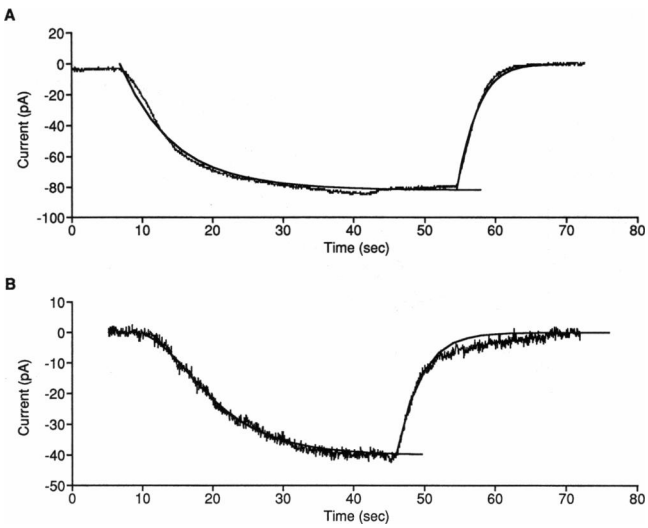

FIGURE 10 Comparison of diffusion coefficients at high and low cGMP concentrations measured in the same bullfrog rod outer segment. $L = 25$ μm. (*A*) Membrane current elicited by 35 μM cGMP before the exposure to Ni^{2+}. The values of the constants $K_{1/2}$ and n were determined to be 46 μM and 1.3, respectively, and the maximum current at 1 mM cGMP was 172 pA. The $J(T)$ templates (thick lines) are scaled by 0.045 s^{-1} and 0.140 s^{-1}, respectively, to fit the rising and falling phases of the current. (*B*) Membrane current elicited by 5 μM cGMP after internal dialysis of the outer segment with 100 μM Ni^{2+} for ~5 min. The values of the constants $K_{1/2}$ and n after exposure to Ni^{2+} were determined to be 9.2 μM and 2.7, respectively, and the maximum current at 100 μM cGMP was 192 pA. The $J(T)$ templates (thick lines) are fitted to the rising and falling phases of the current with α values of 0.058 s^{-1} and 0.050 s^{-1}, respectively.

TABLE 2 Comparison of cGMP diffusion coefficients at high and low cGMP concentrations, measured in the same rod outer segment

Species	cGMP diffusion coefficient ($\times 10^{-8}$ cm^2 s^{-1})	
	High cGMP (20–1000 μM)	Low cGMP (5–10 μM)
Bullfrog	47 ± 10	58 ± 20
Salamander	50 ± 12	55 ± 10

The diffusion coefficients at high cGMP were obtained in the absence of Ni^{2+}; those at low cGMP were obtained in the presence of Ni^{2+}. Each number represents the average data from two outer segments.

segments is obviously the baffling by the membranous disks, or the tortuosity factor. This factor of six to seven that we obtained is in broad agreement with the fivefold difference between the lateral and longitudinal diffusion coefficients of 6-carboxyfluorescein measured by Phillips and Cone (1985).

How is the tortuosity factor related to the physical structure of the outer segment? The ratio of the diffusion coefficient along the outer segment, D, to that in aqueous solution, D_{aq}, due to the baffling can be expressed as:

$$\frac{D}{D_{aq}} = \frac{F_A}{F_V} \tag{14}$$

where F_A and F_V are the outer segment cross-sectional area and volume, respectively, available for diffusion (Lamb et al., 1981; Olson and Pugh, 1993). From electron micro-

graphs provided by A. P. Mariani (see also Brown et al., 1963; Tsukamoto, 1987), Olson and Pugh (1993) concluded that $F_A = 0.014$ and $F_V = 0.5$, so that the diffusion coefficient in the outer segment would be expected to be ~30 times lower than in aqueous solution. This expected value is six times lower than our measurements. One explanation for this discrepancy would be that truncation damages the structural integrity of the outer segment and somehow increases the F_A/F_V ratio. We consider this unlikely, because the measured diffusion coefficient did not change appreciably even with repeated truncations (Fig. 7*B*). Also, the measured diffusion coefficient did not vary considerably from cell to cell, as might be expected from random damage. A more likely explanation is that an F_A value of 0.014 is an underestimate due to dehydration of tissue prepared for electron microscopy. For example, freeze-etching studies have suggested F_A values higher than those obtained from sections, being as high as 0.04 (Rosenkranz, 1977). At the same time, although the aqueous volume in rod outer segments is ~0.5 (Sidman, 1957; Blaurock and Wilkins, 1969), not all interdiskal space may be accessible to cGMP diffusion. Indeed, a study by Cohen (1968) has indicated that barium sulfate can diffuse at the disk perimeter and in the incisure space but not in the interdiskal space. If cGMP diffusion is restricted in the same way, F_V can be significantly less than 0.5. In conclusion, the actual F_A/F_V ratio can be larger than 0.03 and would support our measurements of the diffusion coefficient.

The diffusion coefficient we report here is also sixfold higher than the upper limit of 10×10^{-8} cm^2 s^{-1} estimated by Cameron and Pugh (1990) and Olson and Pugh (1993). Both of these studies utilized a whole cell recording pipette to introduce cGMP or cGMP analogues into a tiger salamander rod or rod outer segment, and employed diffusion theory to calculate the diffusion coefficient. Their method has the advantage of maintaining the structural integrity of the outer segment, but the diffusion models they used were necessarily more complex and involved additional parameters that had to be estimated or assumed to derive the cGMP diffusion coefficient.

Our experiments with Ni^{2+} indicate no significant effect of buffering on cGMP diffusion at concentrations between 5 μM and 1 mM. It is possible that soluble cGMP binding sites have washed out of the truncated rod outer segment, although no such soluble sites have been reported (see Cote and Brunnock, 1993). More than 90% of the total cGMP in the rod outer segment is bound (Nakatani and Yau, 1988b; see also Woodruff and Fain, 1982 and Cote et al., 1984), most of which is apparently associated with noncatalytic binding sites on the cGMP-phosphodiesterase, a membrane-associated enzyme. These sites have submicromolar affinities for cGMP (Yamazaki et al., 1980; Cote and Brunnock, 1993; Cote et al., 1994), too high to affect the diffusion coefficient under our conditions. Also, the light-dependent decrease in the affinity of these sites (Cote et al., 1994) would not have influenced our measurements, which were carried out in darkness. These binding sites might affect the diffusion of cGMP in the light.

We thank Drs. R.-C. Huang, J. M. Corless, and E. N. Pugh, Jr. for helpful discussions and suggestions; in particular, Dr. E. N. Pugh, Jr. has brought to our attention possible concerns of space-clamp failure, as well as literature on rod outer segment anatomy. Drs. R. H. Cote, M. D. Bownds, and V. Y. Arshavsky kindly provided us with a preprint of their work.

This work was supported by National Institutes of Health grant EY06837. Y. Koutalos held a postdoctoral fellowship from the Fight for Sight Research Division of the National Society to Prevent Blindness, awarded in memory of Mary E. and Alexander P. Hirsch.

REFERENCES

Baylor, D. A., T. D. Lamb, and K.-W. Yau. 1979a. The membrane current of single rod outer segments. *J. Physiol.* 288:589–611.

Baylor, D. A., T. D. Lamb, and K.-W. Yau. 1979b. Responses of retinal rods to single photons. *J. Physiol.* 288:613–634.

Blaurock, A. E., and M. H. F. Wilkins. 1969. Structure of frog photoreceptor membranes. *Nature.* 223:906–909.

Bowen, W. J., and H. L. Martin. 1964. The diffusion of adenosine triphosphate through aqueous solutions. *Arch. Biochem. Biophys.* 107:30–36.

Brown, P. K., I. R. Gibbons, and G. Wald. 1963. The visual cells and visual pigment of the mudpuppy, *Necturus. J. Cell Biol.* 19:79–106.

Cameron, D. A., and E. N. Pugh, Jr. 1990. The magnitude, time course and spatial distribution of current induced in salamander rods by guanine nucleotides. *J. Physiol.* 430:419–439.

Carslaw, H. S., and J. C. Jaeger. 1959. Conduction of Heat in Solids, 2nd ed. Oxford University Press, Oxford.

Cervetto, L., L. Lagnado, R. J. Perry, D. W. Robinson, and P. A. McNaughton. 1989. Extrusion of Ca from rod outer segments is driven by both sodium and potassium gradients. *Nature.* 337:740–743.

Cohen, A. I. 1968. New evidence supporting the linkage to extracellular space of outer segment saccules of frog cones but not rods. *J. Cell Biol.* 37:424–444.

Cote, R. H., M. S. Biernbaum, G. D. Nicol, and M. D. Bownds. 1984. Light-induced decreases in cGMP concentration precede changes in membrane permeability in frog rod photoreceptors. *J. Biol. Chem.* 259:9635–9641.

Cote, R. H., M. D. Bownds, and V. Y. Arshavsky. 1994. cGMP binding sites on photoreceptor phosphodiesterase: role in feedback regulation of visual transduction. *Proc. Natl. Acad. Sci. USA.* 91:4845–4849.

Cote, R. H., and M. A. Brunnock. 1993. Intracellular cGMP concentration in rod photoreceptors is regulated by binding to high and moderate affinity cGMP binding sites. *J. Biol. Chem.* 268:17190–17198.

Detwiler, P. B., and M. P. Gray-Keller. 1992. Some unresolved issues in the physiology and biochemistry of phototransduction. *Curr. Opin. Neurobiol.* 2:433–438.

Huang, R.-C., and R. Gillette. 1991. Kinetic analysis of cAMP-activated Na^+ current in the molluscan neuron: a diffusion-reaction model. *J. Gen. Physiol.* 98:835–848.

Karpen, J. W., R. L. Brown, L. Stryer, and D. A. Baylor. 1993. Interactions between divalent cations and the gating machinery of cyclic GMP-activated channels in salamander retinal rods. *J. Gen. Physiol.* 101:1–25.

Koutalos, Y., and K.-W. Yau. 1993. A rich complexity emerges in phototransduction. *Curr. Opin. Neurobiol.* 3:513–519.

Lagnado, L., and D. Baylor. 1992. Signal flow in visual transduction. *Neuron.* 8:995–1002.

Lamb, T. D., P. A. McNaughton, and K.-W. Yau. 1981. Spatial spread of activation and background desensitization in toad rod outer segments. *J. Physiol.* 319:463–496.

Nakatani, K., and K.-W. Yau. 1988a. Calcium and magnesium fluxes across the plasma membrane of the toad rod outer segment. *J. Physiol.* 395: 695–729.

Nakatani, K., and K.-W. Yau. 1988b. Guanosine 3′,5′-cyclic monophosphate-activated conductance studied in a truncated rod outer segment of the toad. *J. Physiol.* 395:731–753.

Olson, A., and E. N. Pugh, Jr. 1993. Diffusion coefficient of cyclic GMP in salamander rod outer segments estimated with two fluorescent probes. *Biophys. J.* 65:1335–1352.

Phillips, E. S., and R. A. Cone. 1985. Cytoplasmic diffusion rates in rod outer segments: how much do the disks slow diffusion along the rod? *Invest. Ophthalmol. Vis. Sci. Suppl.* 26:168 (ARVO Abstract).

Pugh, E. N., Jr., and T. D. Lamb. 1993. Amplification and kinetics of the activation steps in phototransduction. *Biochim. Biophys. Acta.* 1141: 111–149.

Rodieck, R. W. 1973. The Vertebrate Retina. Freeman and Company, San Francisco.

Rosenkranz, J. 1977. New aspects of the ultrastructure of frog rod outer segments. *Int. Rev. Cytol.* 50:25–158.

Sidman, R. L. 1957. The structure and concentration of solids in photoreceptor cells studied by refractometry and interference microscopy. *J. Biophys. Biochem. Cytol.* 3:15–31.

Tsukamoto, Y. 1987. The number, depth and elongation of disc incisures in the retinal rod of Rana catesbeiana. *Exp. Eye Res.* 45:105–116.

Woodruff, M. L., and G. L. Fain. 1982. Ca^{2+}-dependent changes in cyclic GMP levels are not correlated with opening and closing of the light-dependent permeability of toad photoreceptors. *J. Gen. Physiol.* 80:537–555.

Yamazaki, A., I. Sen, M. W. Bitensky, J. E. Casnellie, and P. Greengard. 1980. Cyclic GMP-specific, high affinity, noncatalytic binding sites on light-activated phosphodiesterase. *J. Biol. Chem.* 255:11619–11624.

Yau, K.-W. 1994. Phototransduction mechanism in retinal rods and cones. *Invest. Ophthalmol. Vis. Sci.* 35:9–32.

Yau, K.-W., and D. A. Baylor. 1989. Cyclic GMP-activated conductance of retinal photoreceptor cells. *Annu. Rev. Neurosci.* 12: 289–327.

Yau, K.-W., and K. Nakatani. 1984. Electrogenic Na-Ca exchange in retinal rod outer segment. *Nature.* 311:661–663.

Yau, K.-W., and K. Nakatani. 1985. Light-suppressible, cyclic GMP-sensitive conductance in the plasma membrane of a truncated rod outer segment. *Nature.* 317:252–255.